

# Fast giant flares in discs around supermassive black holes

G. V. Lipunova<sup>1,2</sup>, A. S. Tavleev<sup>3</sup>, and K. L. Malanchev<sup>4,5</sup>

<sup>1</sup> Max-Planck-Institut für Radioastronomie, Auf dem Hügel 69, 53121 Bonn, Germany  
e-mail: gvlipunova@gmail.com

<sup>2</sup> Sternberg Astronomical Institute, Moscow M. V. Lomonosov State University, 13 Universitetski pr., Moscow, 119992, Russia

<sup>3</sup> Institut für Astronomie und Astrophysik, Kepler Center for Astro and Particle Physics, Universität Tübingen, Sand 1, 72076 Tübingen, Germany

<sup>4</sup> McWilliams Center for Cosmology & Astrophysics, Department of Physics, Carnegie Mellon University, Pittsburgh, PA 15213, USA

<sup>5</sup> Department of Astronomy, University of Illinois at Urbana-Champaign, 1002 W. Green St., IL 61801, USA

April 15, 2024

## ABSTRACT

**Aims.** We study the thermal stability of non-self-gravitating turbulent  $\alpha$  discs around supermassive black holes (SMBHs) to test a new type of high-amplitude active galactic nuclei (AGN) flares.

**Methods.** On calculating discs structures, we compute the critical points of stability curves for discs around SMBH, which cover a wide range of accretion rates and resemble the shape of a  $\xi$  curve.

**Results.** We find that there are values of the disc parameters that favour the transition of a disc ring from a recombined cool state to a hot, fully ionised, advection dominated, geometrically thick state with higher viscosity parameter  $\alpha$ . For SMBH with masses  $\sim 10^6 - 10^8 M_\odot$ , such a flare can occur in the geometrically thin and optically thick neutral disc with convective energy transfer through the disc thickness surrounding a radiatively inefficient accretion flow. When self-gravity effects are negligible, the duration of a flare and the associated mass exhibit a positive correlation with the truncation radius of the geometrically thin disc prior to the flare. According to our rough estimates,  $\sim 4 - 3000 M_\odot$  can be involved in a giant flare, i.e. can be accreted or entrained with an outflow lasting 1 to 400 years, if the flare is triggered somewhere between 60 and 600 gravitational radii in a disc around SMBH with  $10^7 M_\odot$ . The accretion rate on SMBH peaks at a super-Eddington value about ten times faster. The peak effective disc temperature at the trigger radius is  $\sim 10^5$  K, but it can be obscured by an optically thick outflow that reprocesses the emission to longer wavelengths.

**Conclusions.** Such a transfer of disc state could trigger a massive outburst, similar to that following a tidal disruption event.

**Key words.** supermassive black holes – accretion discs – bursts

## 1. Introduction

Disc instability is believed to be one of the underlying causes of transient events in binary systems with accretion discs. For dwarf and X-ray novae, a well-studied scenario of outbursts, the Disc Instability Model (DIM, see e.g., Hameury 2020, and references therein) has been developed, according to which the non-monotonic opacity behaviour related to the partial ionization of hydrogen drives the thermal-viscous instability. Admittedly, discs in active galactic nuclei (AGNs) can undergo viscous-thermal instabilities too (e.g., Mineshige & Shields 1990; Siemiginowska et al. 1996; Menou & Quataert 2001a; Janiuk et al. 2004).

The outburst mechanism can be suitably illustrated using the relationship between the effective temperature or the accretion rate  $\dot{M}$  and the surface density  $\Sigma$  (the disc-thickness-integrated bulk density), – S-curve, see, e.g., Fig. 1 or figure 4 in the review by Lasota (2016) (also Meyer & Meyer-Hofmeister 1981; Smak 1984b). The S-curves are obtained by solving the disc equations in  $z$ -direction (vertical structure equations). If the parameters of a particular ring in a disc fall on the negative branch of the S-curve, the ring is in an unstable state. The ionisation instability that drives the DIM occurs at temperatures  $\sim 10^4$  K.

For example, in low-mass X-ray binaries, matter from a normal star may accumulate in a slowly expanding torus around a compact object. As the mass accumulates, the temperature grad-

ually rises and ionisation of the hydrogen eventually becomes possible. Then a notorious opacity dependence on temperature allows a thermal instability (see e.g. Faulkner et al. 1983). The disc matter becomes hotter and ionised, the viscous time shortens and a mass redistribution leads to the enhanced accretion on the central object and to the electromagnetic flare.

At higher temperatures, the radiation-dominated regime comprises another negative branch of the  $\dot{M}(\Sigma)$  dependence for larger accretion rates, close to the Eddington limit. This regime is thermally and viscously unstable as well (Lightman & Eardley 1974; Shakura & Sunyaev 1976; Piran 1978). A hotter positive-slope branch emerges at even higher accretion rates when photon trapping with the radially moving matter (advection) acts as an energy sink at each radius (Abramowicz et al. 1988, 1995; Björnsson et al. 1996). A corresponding limit cycle behaviour for black hole discs with accretion rates close to Eddington has been proposed (Janiuk & Czerny 2011; Czerny 2019, and references therein).

In the present work we study the stability curves for discs around SMBHs in a wide range of accretion rates. These stability curves resemble letter ‘ $\xi$ ’ and have two unstable branches, connected to partial-ionization instability and radiation-pressure instability, and four critical values of the surface density. We find a new scenario of disc heating, triggered by the ionisation instability, which can only occur in a disc around a SMBH and

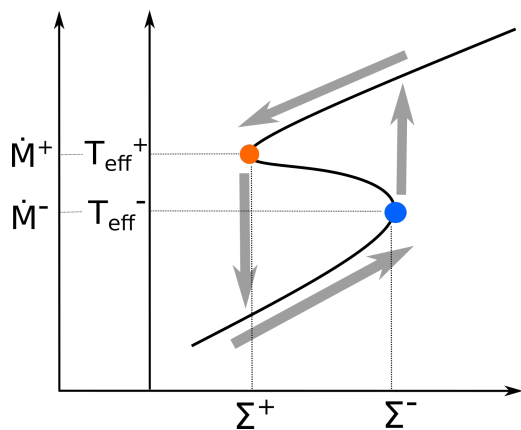


Fig. 1: General S-curve at some radius in accretion disc. The limit cycle instability is shown schematically: on the lower branch the mass accumulates, on the upper branch the mass flows out of a ring.

is based on the assumption that the turbulent  $\alpha$ -parameter becomes higher in ionised discs. The relative positions of the critical points on the stability curve in the case of SMBH allow a disc ring heated by ionisation instability to bypass the gas pressure dominated regime and continue to heat until advection stabilises the disc. This leads to a huge increase in the accretion rate, by a factor of  $10^5 - 10^6$ . Such a transition is likely to induce the super-Eddington state, when strong outflows are produced. The large semi-thickness of an optically thick advection-dominated disc explains a comparatively short flare duration.

We expect such flares to be observationally similar to tidal disruption events (TDE), except for the asymmetric manifestations. According to our toy-model estimates, the giant flares can be more powerful and longer than the typical average TDE. Assuming a constant supply of matter from a galaxy to the central SMBH, giant flares may be about ten times less frequent than current observed rate of TDEs. The emission from the initial heating is likely to be in the extreme ultraviolet and optical diapason, followed by soft X-rays, which may be strongly attenuated, as is usually expected from the outflowing accretion discs in the unfortunate geometrical situation.

In §2 we describe an analysis that can be carried out using stability curves for discs around SMBHs. The conditions necessary for giant flares and their basic properties are presented in §3 and §4. We discuss the implications of the proposed mechanism in §5 and we summarise in §6.

## 2. Local stability curves of SMBH discs

Let us first briefly consider an outburst due to thermal-viscous instability using S-curves. We neglect for a while a possible change of the turbulent parameter  $\alpha$ .

For each radius in a quasi-stationary disc, a proper S-curve can be constructed, see Fig. 2. As we can see, the critical surface densities  $\Sigma^-$  and  $\Sigma^+$  at each radius (namely, the abscissas of the turns, – the blue and orange points, – of the S-curve in Fig. 2) bound an interval of the surface density. If the actual  $\Sigma$  of a ring were to lie within this interval, this would mean that the ring would be capable of transitioning to an alternative thermal state (another positive branch) if the thermal equilibrium were disturbed. If the heating is triggered at  $r_1$ , the heating wave could reach to  $r_3$  but no further, since the disc had the minimum possible density allowing ionization of matter there.

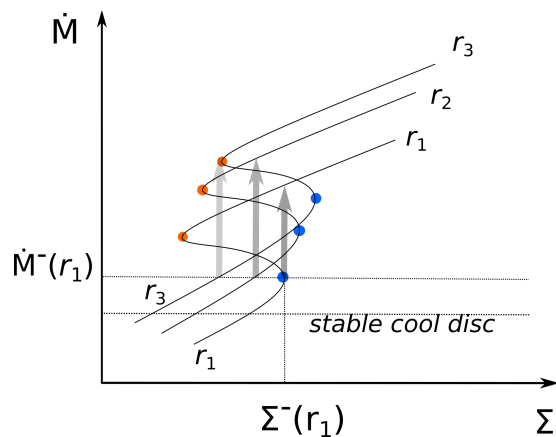


Fig. 2: S-curves at different radii  $r_1 < r_2 < r_3$ , shown schematically for ionization instability. When the accretion rate is very low, the whole disc is stable and cool (the bottom line on the plot). If the surface density exceeds the critical value at the innermost radius  $r_1$ , a heating wave, indicated by grey arrows, starts outwards, potentially reaching  $r_3$ .

At higher temperatures, an unstable radiation-dominated regime and a stable advective regime of accretion emerge. The analytic relations between the accretion rate and surface density could be obtained for these branches. When the radiation pressure dominates over the gas pressure in the geometrically thin disc (the so-called A-zone, Shakura & Sunyaev 1973), the height-integrated viscous stress can be expressed algebraically from  $\Sigma$  using the vertical structure equations (Lightman & Eardley 1974). Here, using the stationary-disc relation between the viscous stress tensor and  $\dot{M}$ , we obtain:

$$\dot{M} = \frac{\Pi_3 \Pi_4^2}{\Pi_1 \Pi_2^2} \frac{32}{9\pi\alpha\omega_K} \left(\frac{L_{\text{edd}}}{GM}\right)^2 \frac{1}{\Sigma_0}, \quad (1)$$

where  $\alpha$  is the turbulent parameter in the disc (Shakura & Sunyaev 1973),  $\omega_K$  is the angular Keplerian velocity,  $M$  is the black hole mass,  $L_{\text{edd}}$  is the Eddington limit

$$L_{\text{Edd}} = \frac{4\pi GMcm_p}{\sigma_T} \simeq 1.25 \cdot 10^{38} \frac{M}{M_\odot} \text{ erg/s} \quad (2)$$

and we adopted  $\Pi$ -parameters from Tavleev et al. (2023, equation 24), which are dimensionless values obtained by solving or averaging the vertical structure of the disc.<sup>1</sup> The Thomson cross section is denoted by  $\sigma_T$  and other symbols have standard meaning.

If the temperature is even higher, for  $\dot{M} \gtrsim \dot{M}_{\text{Edd}}$ , the central part of the disc becomes geometrically thick (a slim disc) and the radial advection starts to play role. Below we use the definition for the Eddington accretion rate:

$$0.1 \dot{M}_{\text{Edd}} c^2 \equiv L_{\text{Edd}}, \quad \dot{M}_{\text{Edd}} \simeq 1.39 \cdot 10^{18} \frac{M}{M_\odot} \text{ g/s}. \quad (3)$$

Combining the equations for hydrostatic balance and viscous energy release (e.g., Tavleev et al. 2023, equations 1 and 2), or using again the  $\Pi$ -parameters, we obtain:

$$\dot{M} = \frac{2\pi}{\Pi_1 \Pi_3} \alpha \sqrt{GMr} \Sigma_0 \left(\frac{z_0}{r}\right)^2. \quad (4)$$

<sup>1</sup> Omitting the solution of the vertical structure leads to all  $\Pi = 1$  as in the approach of Shakura & Sunyaev (1973).

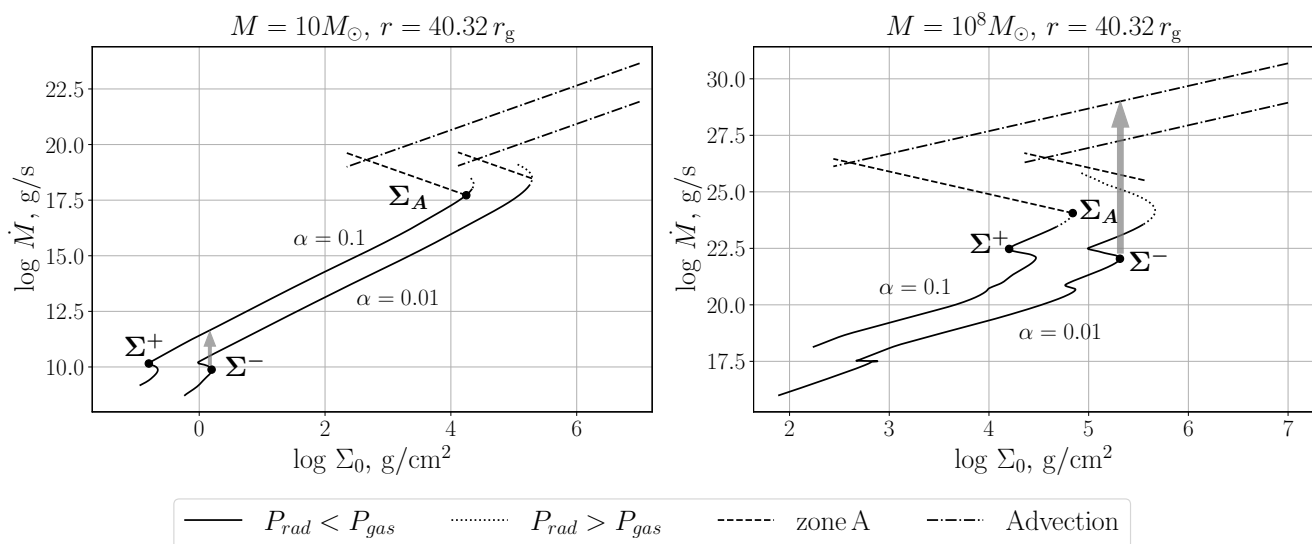


Fig. 3: Stability curves for discs around a stellar-mass BH (left panel) and a SMBH (right panel). Analytical relation (1) for A-zone (dashed) and analytical relation (4) for the advection zone (dash-dotted) are depicted. In each panel the left and right  $\xi$ -curves are calculated for different turbulent parameters  $\alpha$ : 0.1 and 0.01 respectively. Critical points  $\Sigma_A$  and  $\Sigma^+$  are marked only on the left  $\xi$ -curves,  $\Sigma^-$  on the right. The indicated value of the turbulent parameter  $\alpha_{\text{cold}} = 0.01$  is assumed to occur below the point  $\Sigma^-$ ; and  $\alpha_{\text{hot}}$ , above the point  $\Sigma^+$ . The arrows schematically show the direction of ring heating due to ionisation instability and  $\alpha$  increment.

The half thickness  $z_0$  should satisfy the energy balance equation, which can be solved together with the radial structure of an advective supercritical disc. In the advective regime the disc semi-thickness saturates and we can roughly assume  $z_0/r \approx 0.5$  (e.g., Lipunova 1999; Lasota et al. 2016). The slope of the  $\dot{M}(\Sigma)$  relation is positive for constant  $z/r$ , implying the viscous stability of the advective zone (see Kato et al. 2008).

### 2.1. Non-stationary discs around SMBH

It has been proposed that in stellar mass systems, the turbulence parameter  $\alpha$  is higher in ionised material discs compared to neutral matter discs (e.g., Smak 1984a; Meyer & Meyer-Hofmeister 2015). We assume different  $\alpha$  for a cold neutral and a hot fully ionised disc, although the decreasing  $\alpha$  in the recombined material in AGN discs has been criticised (Menou & Quataert 2001b). Janiuk et al. (2004) studied the magnetic Reynolds and ambipolar diffusion numbers and found that they appear to exceed the critical values required for sustained turbulence unless the accretion rate is very low. We can speculate that  $\alpha$  might still depend on the degree of ionisation, as shown for protoplanetary discs by Landry et al. (2013); see also discussion in §2.1 of Hameury et al. (2009).

Examples of stability curves for a stellar-mass black hole and a SMBH are shown in Fig. 3. To calculate S-curves for states of the optically-thick and geometrically thin disc around SMBHs, we use our publicly available code (Tavleev et al. 2023). The upper branches are depicted according to Eqs. (1) and (4), by dashed and dot-dashed lines, respectively.

The difference between the S-curves of the stellar-mass BH and the SMBH is easy to see. For a very massive central black hole, the maximum critical surface density in the cold disc  $\Sigma^-$  around the SMBH for lower  $\alpha_{\text{cold}}$  is larger than the maximum critical density  $\Sigma_A$  of the geometrically thin hot ionised disc for larger  $\alpha_{\text{hot}}$ .

This can lead to a ‘giant flare’ event. If the surface density in the cold state of a SMBH disc exceeds a critical maximum value

the heating instability can lead to a direct transition of the ring to an advective state, skipping a ‘thin ionised’ state. This transition occurs on a thermal timescale. We cannot calculate the course of such heating in this paper. This is generally very difficult to do at the current level of disc simulation. However, the central point of the proposed mechanism is the assumption that if the ring in the diagram ( $\Sigma$ ,  $T$ ) turns out to be at such a large surface density  $\Sigma$  that there is a stable solution only at high temperature, then the ring should transfer to this hot state if it does not lose its density faster. This is similar to the classic mechanism in the DIM model.

An important caveat here is that Figure 3 is constructed for a quasi-stationary disc. Firstly, a quasi-stationary viscous radial torque distribution is assumed. Secondly, a sufficient time must elapse before the disc ‘settles’ and a state on the S-curve can be realised. In the case of a geometrically thin disc, this time must be of the order of the thermal time. In the case of a slim advective disc, whose energy balance is not local, this time can be longer, apparently, of order of the viscous time. This follows from the fact that the quasi-stationary accretion state at the highest positive branch can be achieved only when the radial transfer of energy is established. For the latter, the disc zone in question has to be already thick and advective. However, because the slim disc is quite thick, the viscous time scale  $(r/z_0)^2 (\alpha \omega_K)^{-1}$  is not much longer than the thermal time  $(\alpha \omega_K)^{-1}$ .

We assume that on the local viscous time scale the slim disc at each radius approaches a state corresponding to a point on the uppermost branch on the S-curve. The heating may be accompanied with an optical flare of a modest magnitude. At the same time, the accretion rate on the central BH starts to increase and its maximum depends on the mass available in the heated state, i.e. on the range of radii where the disc has switched to the advective state.

The evolution of the accretion rate on the SMBH depends on how the size of the advective zone decreases with time and on the outflows from the disc surface. The duration of the flares can be estimated as the viscous time at the maximum radius  $r_{\text{max}}$  of

the advective zone:

$$t_{\text{vis}} = \frac{r_{\text{max}}^2}{v_t} = \frac{3}{2} \frac{1}{\alpha \omega_K} \left( \frac{z_0}{r} \right)^{-2} \Pi_1. \quad (5)$$

This time can be an order or two longer than the orbital time  $1/\omega_K$  because  $\alpha \sim 0.1$  and  $\Pi \sim \text{few}$ . If one approximates a light curve by the exponential law, the  $e$ -folding decay time  $t_{\text{exp}} \approx 0.4 t_{\text{vis}}$  is as follows:

$$t_{\text{exp}} \approx 60^d \left( \frac{\alpha}{0.1} \right)^{-1} \left( \frac{z_0}{r} \right)^{-2} \left( \frac{r_{\text{max}}}{100 r_g} \right)^{3/2} \left( \frac{M}{10^7 M_\odot} \right) \quad (6)$$

see Appendix A, where

$$r_g = 2GM/c^2. \quad (7)$$

This time is much shorter than the viscous evolution time in the geometrically thin disc around the SMBH due to the fact that  $z_0/r \sim 1$  in the advective regime and  $z_0/r \sim 10^{-3}$  for a thin disc.

In the following section, we abandon the analytical approximations for the branches of the  $\xi$ -curves and calculate them numerically. We continue to call them S-curves (stability-curves).

## 2.2. Turning points of the stability curves

The critical values of the stability curves affect the possibility of a giant flare and its amplitude. To find these values,

$$\begin{aligned} \Sigma^- &= \Sigma^-(r, \alpha_{\text{cold}}), & \Sigma^+ &= \Sigma^+(r, \alpha_{\text{hot}}), \\ \Sigma_A &= \Sigma_A(r, \alpha_{\text{hot}}), & \Sigma_{\text{adv}} &= \Sigma_{\text{adv}}(r, \alpha_{\text{hot}}), \\ \alpha_{\text{cold}} &= 0.01, & \alpha_{\text{hot}} &= 0.1, \end{aligned} \quad (8)$$

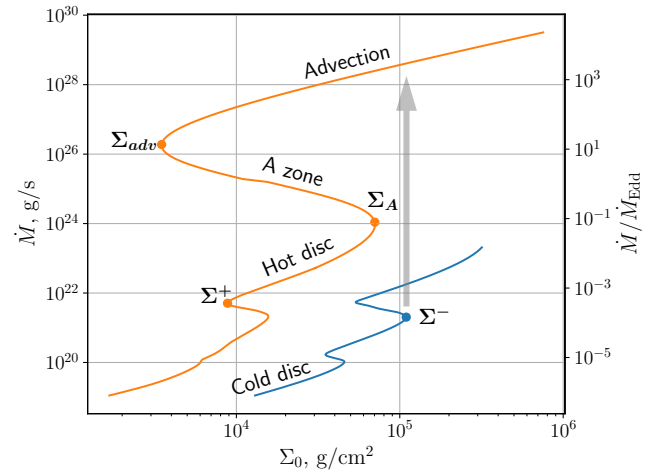
we construct a set of S-curves (see example in Fig. 4a) for different SMBH masses.

The S-curves for regimes when the gas pressure dominates are calculated using the open code `DISCVERST` by Tavleev et al. (2023). In the radiation-pressure dominated regime, the code of Lipunova (1999) is used, applying a conservative scheme, i.e. without wind. While the super-Eddington accretion disc is expected to launch powerful winds, the critical values of the turning points are not significantly affected by this. The wind has been proposed to start when the total bolometric luminosity of the disc exceeds the Eddington value, shown on the right vertical axis in Fig. 4a, i.e. on the upper positive branch. The code by Lipunova (1999) calculates the radial structure of a disc with the optional advection-dominated super-Eddington central zone, assuming the constant dimensionless parameters  $\Pi_{1..4}$ , characterizing the vertical structure (Ketsaris & Shakura 1998; Tavleev et al. 2023). We stitch the radial structure obtained in the two codes at a point in the interval between  $\Sigma^+$  and  $\Sigma_A$  (marked as ‘Hot disc’), using the  $\Pi_{1..4}$ -values calculated in the `DISCVERST` code at this point. To construct the global S-curves (like shown in Figs. 4), we calculate the radial structure for many values of  $\dot{M}$ .

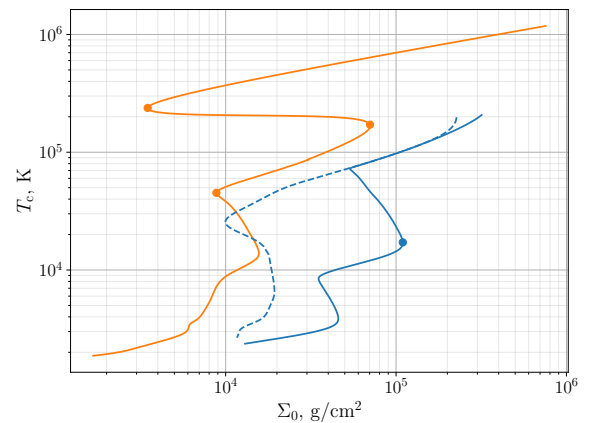
Resulting dependencies of the critical values (8) are shown for one SMBH mass in Fig. 5. Only one curve  $\Sigma^-$  is calculated with  $\alpha = \alpha_{\text{cold}}$ , and others, with  $\alpha = \alpha_{\text{hot}}$ . A giant flare can happen if  $\Sigma^-(\alpha_{\text{cold}}) > \Sigma_A(\alpha_{\text{hot}})$ .

In Fig. 4b we also show the stability for a disc calculated without convection by the dashed line. Cannizzo & Reiff (1992) noted that ignoring convection reduces the critical surface density. Our values of  $\Sigma^-$  agree well with the results of Hameury et al. (2009) with convection.

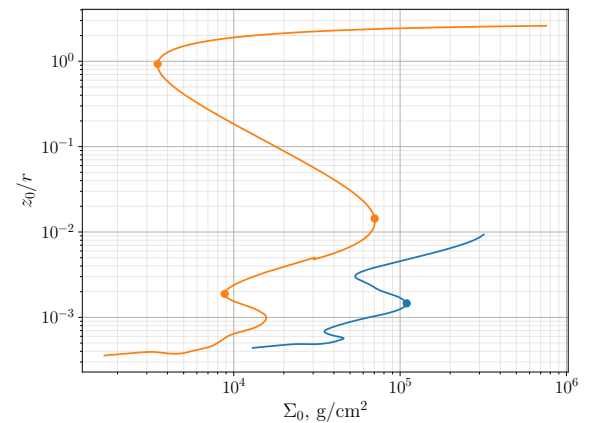
The semi-thickness of the advective disc is greater than 1 in Fig. 4c. This can be attributed to the approximate character



(a) Accretion rate in absolute units shown on the left axis and in the Eddington rates (3), on the right.



(b) Temperature  $T_c$  in the symmetry plane. The dashed line shows the S-curve for  $\alpha_{\text{cold}}$  without convection.



(c) Relative semi-thickness  $z_0/r$ .

Fig. 4: S-curves for  $10^7 M_\odot$  at  $r = 100r_g$  for two values of turbulent parameter  $\alpha_{\text{cold}} = 0.01$  (blue) and  $\alpha_{\text{hot}} = 0.1$  (orange). The branches ‘A-zone’ and ‘Advection’ were calculated using the code from Lipunova (1999).

of the vertical structure approach in the code based on that of (Lipunova 1999) (in the original paper  $\Pi_1 = 1$ , which decreases the thickness). Here we keep  $\Pi_1$  constant ( $\sim \text{few}$ ) along the upper S-curve as we are most interested in calculating  $\Sigma_A$ . In the following analysis, see §4, we assume a value of  $z_0/r = 0.5$  for the thickness of the advective slim disc.

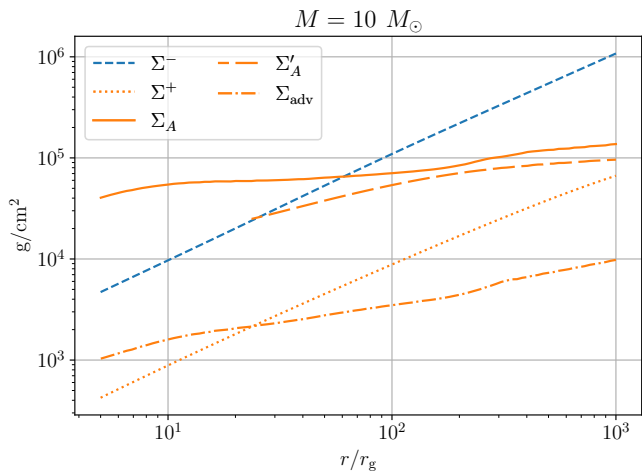


Fig. 5: Critical values of surface density (8) for  $M = 10^7 M_\odot$ . Viscous parameter is  $\alpha_{\text{cold}} = 0.01$  for  $\Sigma^-$  (the blue line) and  $\alpha_{\text{hot}} = 0.1$  in all other dependencies (orange lines). Relations  $\Sigma_A$  and  $\Sigma'_A$  show results of different codes, see §2.2.

In Fig. 5, the turning points corresponding to change between the gas- and radiation-pressure-dominated accretion regime are presented as obtained in two alternative ways ( $\Sigma_A$  and  $\Sigma'_A$ ). Generally, the vertical structure code `DiscVERST` (which includes convection and tabular opacities and calculates  $\Pi_{1,4}$  values) has numerical difficulties when the radiation pressure is large, but in some cases we have managed to obtain the turning points  $\Sigma'_A$ . We see that at those radii, when we have  $\Sigma'_A$ , – result of `DiscVERST`, – it is less than  $\Sigma_A$  and, thus, cannot hinder the proposed mechanism. For further analysis we will use the  $\Sigma_A(r)$  dependence, keeping in mind its approximate character.

### 2.3. Thermal-viscous instability in the disc around SMBH

Consider the case of BH with  $10^7 M_\odot$ . In Fig. 6a, we show the surface density distributions  $\Sigma_{\text{stat}}(r)$  for several values of accretion rate in a quasi-stationary disc around the SMBH. In the panels (b) and (c), we cut the surface density distributions at the intersections with  $\Sigma^-(r)$ . The radial dependencies of the critical values of S-curves are plotted too. The similar plots for other SMBH masses can be found in Fig. A.4.

In the quiescent epoch, as the mass accumulates in the disc due to income of the galactic matter, in its innermost parts (shown in Fig. 6a) the accretion rate  $\dot{M}$  can slowly increase. We imagine that the grey curves change successively in time, replacing each other in order from bottom to top. In reality, the accretion rate probably increases with radius in a quiescent disc. Consequently, realistic  $\Sigma(r)$  would have more positive slope (compare, for example with figure 5b in Hameury et al. 1998). This observation does not lead to qualitative changes in the picture. It can be kept in mind, though, that the accretion rates, indicated in Fig. 6, correspond to the accretion rate at the inner disc radius.

As long as  $\dot{M} \lesssim 10^{-7} \dot{M}_{\text{edd}}$ , the whole disc is in the stable cold state (this accretion rate roughly corresponds to the intersection of  $\Sigma^-(r)$  with a grey curve  $\Sigma_{\text{stat}}(r)$  at the inner disc edge). Nowhere in the disc does the surface density and temperature reach values where hydrogen ionisation triggers the instability.

When the quasi-stationary accretion rate exceeds  $\sim 10^{-7} \dot{M}_{\text{edd}}$ , the surface density  $\Sigma_{\text{stat}}$  becomes greater than  $\Sigma^-$  near the inner edge of the disc (see Fig. 6b). At this radius

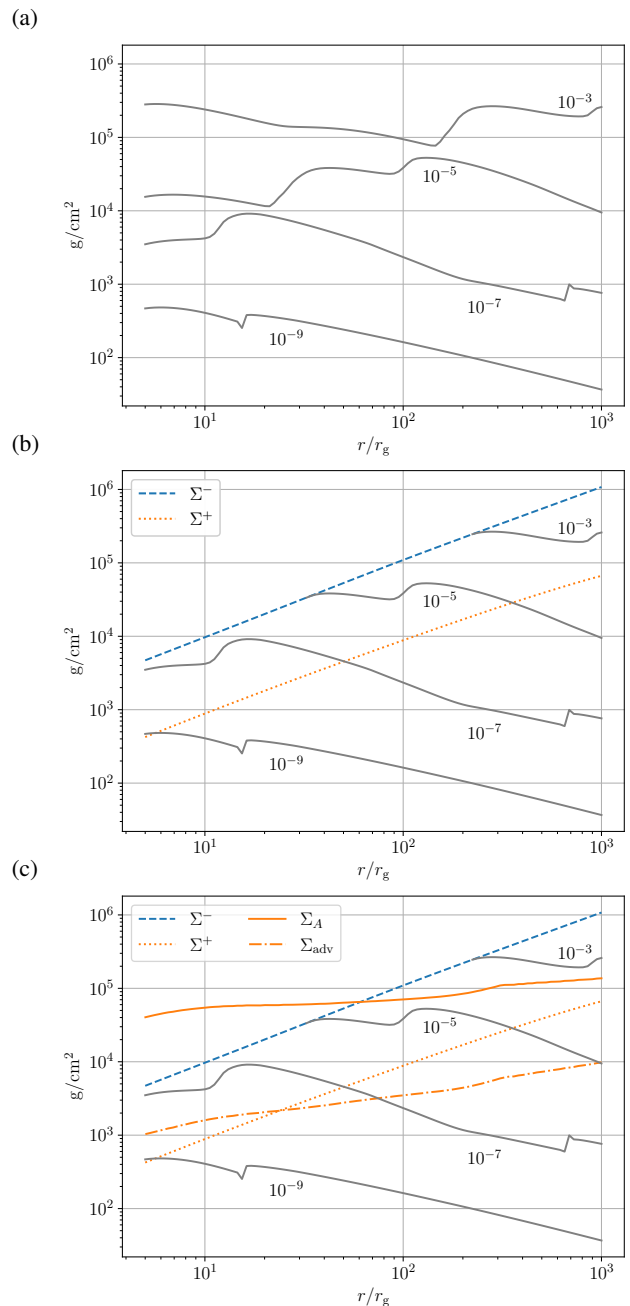


Fig. 6: (a) Quasi-stationary surface density  $\Sigma_{\text{stat}}(r)$  for  $M = 10^7 M_\odot$  and  $\alpha = \alpha_{\text{cold}}$  at several values of  $\dot{M}$  (indicated in the panels in units of  $\dot{M}_{\text{Edd}}$ ); (b) Radial distributions of the critical points  $\Sigma^+$  for  $\alpha_{\text{hot}}$  and  $\Sigma^-$  for  $\alpha_{\text{cold}}$  together with the stationary distributions. The latter are shown only for  $\Sigma_{\text{stat}} < \Sigma^-$ ; (c) Added are the radial dependencies of the critical points  $\Sigma_A$  and  $\Sigma_{\text{adv}}$  for  $\alpha_{\text{hot}}$ . In all panels,  $\alpha_{\text{cold}} = 0.01$  (blue) and  $\alpha_{\text{hot}} = 0.1$  (orange).

$\Sigma^- < \Sigma_A$ , see Fig. 6c. This means that the outburst can occur in the classical framework of the DIM model. There will be a transition from the lower cool branch to the upper hot branch near the inner edge of the disc ( $\Sigma$  is between  $\Sigma^+$  and  $\Sigma_A$ ), and the hot front will start to propagate outwards. A rebrightening of the disc also occurs. The accretion rate to the SMBH increases, resulting in a slow outburst with the characteristic time  $t_{\text{vis}} \sim 5 \cdot 10^4$  yr, found from (5) by substituting  $z_0/r \sim 0.002$  (cf. Fig. 4c) and  $r_{\text{max}} \sim 60 r_g$ . (Value  $r_{\text{max}}$  can be very roughly

estimated as the intersection of the grey curve for  $10^{-7}\dot{M}_{\text{edd}}$  and the curve  $\Sigma^+(r)$ , see Fig. 6b).

At the end of the outburst, as the cooling front moves towards the disc centre and the disc surface density falls below  $\Sigma^+$ , the disc moves to the lower cold branch of the stability curves at each radius. The transition to the lower stable branch is actually possible for any  $\Sigma$  in the interval from  $\Sigma^+$  to  $\Sigma^-$ . In that respect the left arrow in Fig. 1 is drawn very tentatively. Due to the external influx of matter, the process can start anew. The time between these flares corresponds to a long viscous time in a geometrically thin cold disc with  $\alpha = \alpha_{\text{cold}}$ .

### 3. Conditions for a ‘giant’ flare

It is believed that to explain the spectral features, evolution and timing of low accretion rate black hole (SMBH and stellar mass) accretion discs, it is necessary to assume that a geometrically thin disc is truncated from the inside and its inner part is replaced by a high temperature and low density accretion flow (see, e.g., Yuan & Narayan 2014; Nemmen et al. 2014).

The absence of a standard disc at small radii means that, compared to the situation considered in §2.3, the quiescent accretion rate can increase to higher values without the disc triggering an instability. This is due to the fact that the surface density in the central region is lower than in the standard disc (while the radial velocity is higher).

For example, consider a disc around  $10^7 M_{\odot}$  black hole with the truncation radius  $R_{\text{trunc}} \sim 40 r_g$ . As can be seen from Fig. 6b, the quiescent accretion rate must exceed  $10^{-5} \dot{M}_{\text{Edd}}$  for an outburst similar to the one described in §2.3 to occur: the ring transfers to ‘Hot disc’ state. In particular, if  $\Sigma$  is close enough to  $\Sigma_A$ , the increased accretion rate from this ring inwards will be such that the inner part of the disc, at  $r < 40 r_g$ , will be in the radiation-pressure instability zone (A zone), potentially driving fluctuations proposed to explain Changing-Look AGN (e.g., Śniegowska et al. 2023).

However, consider a situation where the truncation radius  $R_{\text{trunc}}$  is larger, so large that a giant flare is produced. For  $M = 10^7 M_{\odot}$  this happens when  $R_{\text{trunc}} \sim 60 r_g$ . This value is determined by the intersection of the curves  $\Sigma^-(r)$  and  $\Sigma_A(r)$ , see panel (c) in Fig. 6.

The truncation radius  $R_{\text{trunc}}$  directly determines the accretion rate before a giant flare, which is the critical value of the accretion rate at the turning point (point  $\Sigma^-$  in Fig. 4a). Figure 7 shows the accretion rate before the flare  $\dot{M}_{\text{before}}$  versus the truncation radius  $R_{\text{trunc}}$  for different SMBH masses. We plot the dependencies only for those truncation radii that are larger than the minimum that allows a giant flare to occur. When the truncation radius is smaller than shown in Fig. 7, the thermal instability results in a ‘normal’ outburst and does not heat the disc to the super-Eddington regime. The maximum value of  $R_{\text{trunc}}$  is determined by the self-gravity limit (see Eq. (10) below).

We can compare the truncation radii with those proposed by models such as the Advection-Dominated Accretion Flow (ADAF; Narayan & Yi 1994) as a replacement for the central standard disc (Narayan 1996; Esin et al. 1997; Poutanen et al. 1997; Dubus et al. 2001; Menou & Quataert 2001a; Janiuk et al. 2004; Hameury et al. 2007; Narayan & McClintock 2008).

To find the transition radius, one needs to consider the physical situation leading to the formation and thermal structure of the transition region (see e.g. Yuan & Narayan 2014, §4.2.2.). Czerny et al. (2004) examined the data from the Broad Line Regions using optical/UV spectra from the Large Bright Quasar Survey and

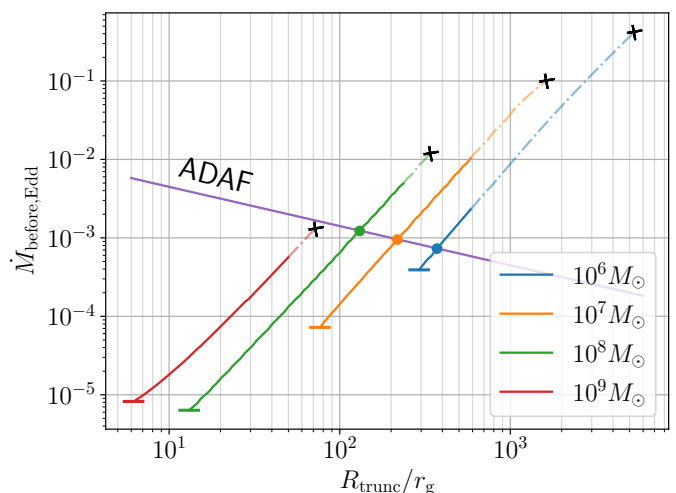


Fig. 7: Accretion rate versus truncation radius of thin disc before giant flare. The predicted dependence between the accretion rate and the ADAF outer boundary (9) is also shown. The crosses mark the radius constraint due to self-gravity following (10). The transparent dashed style indicates the  $R_{\text{trunc}}$  region excluded from further analysis.

found evidence for a ‘strong ADAF principle’: the standard geometrically thin solution is chosen by the disc only if it is the only solution available for certain  $\Sigma$ . Accordingly, an estimate of the radius of the boundary between the ADAF and the standard disc (Abramowicz et al. 1995; Czerny et al. 2004; see further references in Śniegowska et al. 2020) is as follows:

$$R_{\text{ADAF}}/r_g \sim 200 \left( \frac{\alpha}{0.01} \right)^4 \left( \frac{\dot{M}}{10^{-3} \dot{M}_{\text{Edd}}} \right)^{-2}. \quad (9)$$

Inverted relation (9) is shown in Fig. 7. Taking the purple ‘ADAF’ line in Fig. 7 as an upper bound, we infer that there is potentially a wide range of parameters that allow giant flares to occur. Obviously, the required accretion rates  $\dot{M}_{\text{before}}$  and  $R_{\text{trunc}}$  depend on the ratio  $\alpha_{\text{hot}}/\alpha_{\text{cold}}$ ; they grow as the ratio decreases.

### 4. Properties of the giant flares

Similar to the DIM scenario, the ring heated by the instability can trigger a transition wave (a heating wave) that moves outwards. How far out can such a wave travel? The maximum possible distance  $R_{\text{out, max}}$  is determined by the condition that  $\Sigma_{\text{stat}}$  there (before the outburst) should not be less than  $\Sigma_{\text{adv}}$  (see Fig. 4a). This can be difficult to achieve in a ‘rapidly changing landscape’ because, for example, viscous evolution occurs on almost the thermal timescale. We suggest that the minimum extent of the heating wave is on the order of  $z_0(R_{\text{trunc}})$ , assuming isotropic heat diffusion.

At a certain radius in the disc, the effects of self-gravity begin to take effect. The distance beyond which the razor-thin disc becomes gravitationally unstable is defined by the following condition (Safronov 1960; Toomre 1964):

$$\frac{\pi G \Sigma}{\omega_K^2 z_0} \geq 1. \quad (10)$$

The behaviour of the disc and  $\Sigma(R)$  beyond  $R_{\text{sg}}$  depend on the cooling and heating mechanisms there. Given the uncertainties

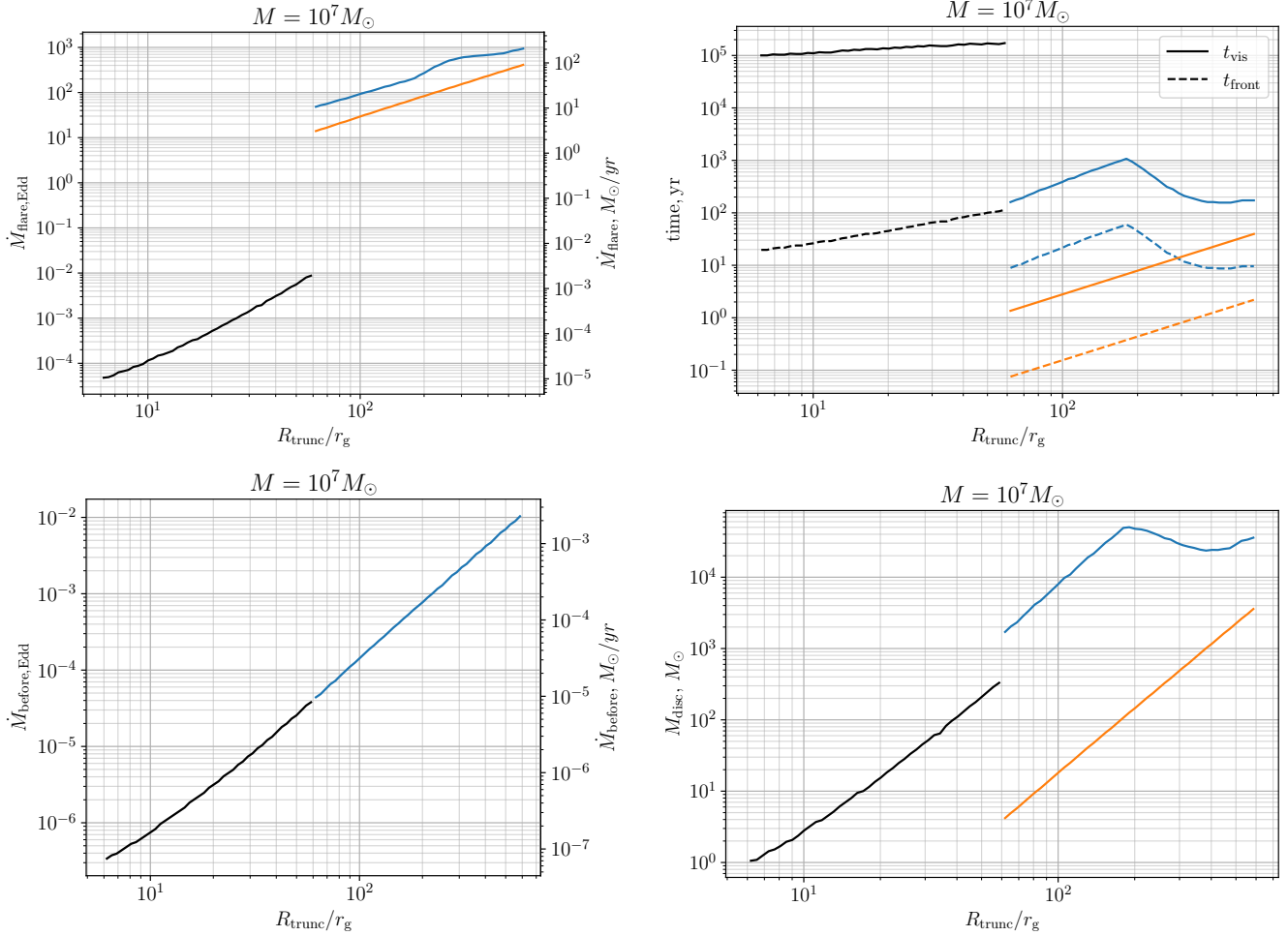


Fig. 8: Outburst properties for normal (black colour) and giant flares (blue and orange) versus inner truncation radius of quiescent geometrically-thin disc. (a) Peak accretion rate (13); (b) Characteristic times, calculated using (11) for the flare evolution before the peak and (5) for the characteristic flare duration; (c) Inner disc accretion rate before the flare; (d) Mass involved in a flare. The blue curves show the upper limit, obtained if the disc is heated to the radius  $R_{\text{out,max}}$ . The orange curves represent the lower limit following assumption  $R_{\text{out}} = R_{\text{trunc}} + z_0$  (see §4);

in the disc structure, which are beyond the scope of the present work, we choose to present the results only for radii less than  $R_{\text{sg}}$ . Also, due to numerical difficulties, we have not calculated flare parameters for  $R_{\text{trunc}}$  very close to  $R_{\text{sg}}$ , nor have we considered radii larger than  $10^3 r_g$ , as our primary focus is on lower estimates. The radii  $R_{\text{trunc}}$  we considered are indicated by the solid intervals of the curves in Fig. 7.

The time before the flare peaks can be estimated as the heating front propagation time (Meyer 1984):

$$t_{\text{front}} = t_{\text{th}} \left( \frac{z_0}{R_{\text{out}}} \right)^{-1} = \frac{1}{\alpha \omega_K(R_{\text{out}})} \left( \frac{z_0}{R_{\text{out}}} \right)^{-1}. \quad (11)$$

For a slim disc, the front time is of order of  $t_{\text{peak}}$  (A.3). It takes time  $t_{\text{peak}}$  for the inner accretion rate to peak for a disc whose size is growing only viscously, e.g. after a heating wave has already reached its limit. The caveat here is that the two estimates are derived from different approaches.

The upper limit of the characteristic flare decay time can be estimated as the viscous time at the outer boundary of the disc involved in the flare  $R_{\text{out}}^2/\nu_t(R_{\text{out}})$ , see Eq. (5). The mass of the

disc that can participate in the flare:

$$M_{\text{disc}} = \int_{R_{\text{trunc}}}^{R_{\text{out}}} 2\pi \Sigma_{\text{stat}} r dr. \quad (12)$$

We neglect here that the surface density changes as the heating front propagates.

Finally, the peak accretion rate can be approximated as the mass divided by the characteristic time, see Eqs. (A.4):

$$\dot{M}_{\text{flare}} = \frac{M_{\text{disc}}(R_{\text{out}})}{R_{\text{out}}^2/\nu_t(R_{\text{out}})}. \quad (13)$$

It should be remembered that a substantial fraction of the ‘heated’ mass is blown away with the outflow. In the slim disc models, the upper limit of the wind loss fraction of the accretion rate has been estimated to be as high as  $\sim 50\%$  (Poutanen et al. 2007).

It is evident that the truncation radius  $R_{\text{trunc}}$  determines  $\Sigma_{\text{stat}}$  and  $\dot{M}_{\text{before}}$  before the flare, as well as the power and duration of the flare itself.

Figures 8 and A.1–A.3 show the calculated parameters of the flares for different SMBH masses: peak accretion rate estimate

Table 1: Peak accretion rate, characteristic duration, and mass involved in giant flares obtained for  $R_{\text{out}} = R_{\text{trunc}} + z_o(R_{\text{trunc}})$ , see §4. For each parameter listed in the first column, we give in the first line the values corresponding to the minimum estimate of  $R_{\text{trunc}}$  and in the second line, a value corresponding to the ADAF prediction of  $R_{\text{trunc}}$  (intersections with the ‘ADAF’ line in Fig. 7).

$M, M_{\odot}$	$10^6$	$10^7$	$10^8$	$10^9$
$\dot{M}_{\text{flare}}, \dot{M}_{\text{Edd}}$	> 30 40	> 10 80	> 6 200	> 10 –
$t_{\text{vis}}, \text{yr}$	> 1 2	> 1 7	> 1 40	> 4 –
$M_{\text{disc}}, M_{\odot}$	> 1 2.5	> 4 230	> 20 $10^4$	> $10^3$ –

(13), front time (11) and viscous time (5), accretion rate in a thin disc before the flare, and the mass involved in a flare. The left sets of points (black; absent for  $10^9 M_{\odot}$ ) represent the values calculated for the ‘normal’ under-Eddington flares (see §2.3). The non-monotonic behaviour of the blue curves for  $R_{\text{trunc}} \gtrsim 200 r_g$  is explained by the fact that, according to our assumption, the maximum radius that the heating wave can reach is limited by the radius of the gravitational instability  $R_{\text{sg}}$ .

Due to the assumed fixed thickness of the slim disc, the ratio between  $t_{\text{vis}}$  and  $t_{\text{front}}$  is about one order everywhere.

For the giant flares, which are faster and more luminous, we plot two sequences: assuming  $R_{\text{out}} = R_{\text{out,max}} \equiv \min(R(\Sigma_{\text{stat}} = \Sigma_{\text{adv}}), R_{\text{sg}})$ , in blue, and  $R_{\text{out}} = R_{\text{trunc}} + z_o(R_{\text{trunc}}) = 1.5 R_{\text{trunc}}$ , in orange. For ‘normal’ flares, we use  $R_{\text{out}} = \min(R(\Sigma_{\text{stat}} = \Sigma^+), R_{\text{sg}})$ , cf. Fig. 2.

Table 1 is a compilation of the flare characteristics for  $R_{\text{out}} = 1.5 R_{\text{trunc}}$ . This case is the least dependent on the radial distribution of the surface density in the quiescent disc and the most conservative estimate.

The effective temperature of the disc at  $R_{\text{trunc}}$  can be estimated from  $\sigma T_{\text{eff}}^4 = \dot{M}_{\text{flare}} GM/r^3$ . Due to the advection effect, we find that the effective temperature can be twice as low; for  $10^6$  and  $10^7 M_{\odot}$ , for  $\dot{M}_{\text{flare}} = 30 - 40$  and  $10 - 80 \dot{M}_{\text{Edd}}$ , respectively,  $T_{\text{eff}} \sim 10^5$  K.

## 5. Discussion

### 5.1. Limits of the local analysis

The main shortcoming of the proposed model is that it is based on a local analysis of the S-curves. Numerical simulations show that the trajectories of the parameters of the disc ring during the development of a flare can be quite complicated, even in the case of ‘normal’ flares, see, e.g., Lasota (2001), figures 11 and 12, Śniegowska et al. (2023), figure 5.

Another possible difficulty is the substantial difference between  $\alpha_{\text{cold}}$  and  $\alpha_{\text{hot}}$  required by the mechanism. Overall, this fits well with the modern paradigm (e.g., Martin et al. 2019). Currently, however, there is a lack of confidence in both the magnitude of alpha and its radial constancy. MHD simulations result in  $\alpha$  varying with the dimensionless disc shear rate (which equals  $3/2$  for a Keplerian disc) and due to the potential contribution of large-scale, mean magnetic fields, which can exist near and inside the inner edge of the disc (Penna et al. 2013). In the magnetically supported disc around  $10^8 M_{\odot}$  in the global radiation MHD simulation  $\alpha = 0.01 - 0.1$  were obtained (Jiang et al. 2019).

Observational constraints for  $\alpha_{\text{hot}}$  in the case of AGN were obtained assuming thermal time-scale of the underlying varia-

tions’ mechanism. On studying the UV/optical spectrum variability of 26 AGN Siemiginowska & Czerny (1989) obtained  $\alpha = 0.001 - 0.1$  and for 49 AGN Starling et al. (2004) obtained  $0.01 - 0.03$ , with  $L/L_{\text{Edd}} = 0.01 - 1$ . Xie et al. (2009) analysed temporal distance between optical light curve maxima of 31 gamma-ray loud blazars with  $L/L_{\text{Edd}} = 0.02 - 0.2$  and got  $\alpha = 0.1 - 0.3$ . An analysis of R-band light curves as of the continuous time stochastic process for 100 quasars provided a lower  $\alpha \sim 0.001$  (Kelly et al. 2009). The stochastic variability in optical and UV is found to be consistent with  $\alpha \sim 0.05$  in 67 AGN (Burke et al. 2021).

### 5.2. Giant flares and Tidal Disruption Events (TDE)

TDEs are invoked to explain bright X-ray, UV and/or optical events in galactic centres lasting months to years (Hills 1975; Rees 1988). If a star passes close enough to an SMBH, and if the tidal forces exerted by the massive object are strong enough, the star can be ripped apart. After returning to the circularisation radius, which is estimated to be twice the tidal radius  $R_{\text{tidal}} = R_{\star} (M/M_{\star})^{1/3}$ ,

$$R_{\text{circ}}/r_g = 2R_{\text{tidal}}/r_g \sim 47 \left( \frac{M}{10^6 M_{\odot}} \right)^{-2/3} \left( \frac{M_{\star}}{M_{\odot}} \right)^{-1/3} \left( \frac{R_{\star}}{R_{\odot}} \right), \quad (14)$$

some debris is thought to form a viscously evolving disc (Cannizzo et al. 1990; Ulmer 1999; Shen & Matzner 2014). The disc of stellar debris, as well as the collisional shock, heats up and emits in a wide range of wavelengths, from optical to X-ray. This sudden increase in brightness is one of the key features used to identify a TDE.

The giant flares involve accretion in the super-Eddington regime, which makes their manifestation similar to that of TDEs (e.g., Shen & Matzner 2014; Komossa 2015; Metzger & Stone 2016; Dai et al. 2018). Similarly, the bolometric luminosity is determined by the disc luminosity, which logarithmically exceeds  $L_{\text{Edd}}$ , plus the emission from the pressure-supported envelope (Sarin & Metzger 2024). The expected wind velocity is also of order of the escape velocity  $\sim \sqrt{2GM/R_{\text{trunc}}} \approx 0.1 c (R_{\text{trunc}}/100 r_g)^{-1/2}$ . As TDEs, giant flares from disc instability can be sources of ultra high-energy cosmic rays (Farrar & Gruzinov 2009).

Most of the TDE observables come from an advanced stage, when the disc is already formed. Accordingly, in many cases, the reason for the super-Eddington mass accretion cannot be definitively established.

In general, the viscous time of giant flares, as shown in Table 1, is not less than one year, which contrasts with the typical duration of most TDEs. However, care should be taken when defining the times for comparison: Eq. (6) shows that the e-folding time of a flare is about 0.4 times less than  $t_{\text{vis}}$  and the rise time is about  $0.1 t_{\text{vis}}$ , see Eqs. (11). It should be noted that longer TDEs sometimes occur (Kankare et al. 2017; Lin et al. 2017; He et al. 2021; Yan & Xie 2018; Zhang 2023; Bandopadhyay et al. 2024). At this stage, we do not want to regard our flare parameters as restrictive, since they are derived from the simplest estimates of the viscous disc evolution model. The parameters given in Table 1 are physically the upper limits for actual giant flares, taking into account that (1) accretion discs with a shrinking outer boundary evolve faster than those with a fixed outer boundary, (2) outflows from radii comparable to the outer disc radius accelerate the evolution <sup>2</sup>.

<sup>2</sup> For  $10^7 M_{\odot}$ , at  $100 r_g$  the slim advective disc cannot exist at  $\lesssim 10 \dot{M}_{\text{Edd}}$  (see Fig. 4a). This shows that the zone of  $z/r \sim 1$ , which is the ‘short



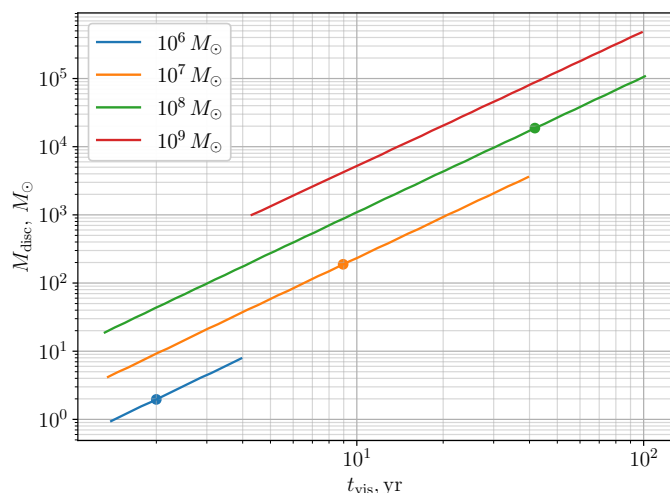


Fig. 9: Disc mass (12) involved in giant flare versus viscosity time (5). The dots mark the values corresponding to the ADAF truncation radius 9, shown in Fig. 7.

Spectral line shapes of TDE are used to extract geometry and kinematics of the photoionised gas. In some works, the interpretation due to the expanding spherical outflow is favoured without invoking the typical prescription of an elliptical disc. (Hung et al. 2019). Kara et al. (2018) found an indication of a  $0.2c$  ionised outflow in ASASSN-14li at early times (about first 40 days), consistent with the O VIII absorption. Using the ionization parameter  $\xi = L_x/(N_H R^2) \sim 10^3$ , the upper limit on the outflow rate  $\dot{M} = m_H N_{Hv_{out}} 4\pi R^2$  can be obtained:  $10^{29} \text{ g/s} \sim 10^3 M_\odot/\text{yr}$ . Matsumoto & Piran (2021) applied the ‘reprocessing-outflow’ model for the optically-thick quasi-spherical wind. By considering observed luminosity, temperature, and outflow velocity, they arrived at the conclusion that the outflows are excessively massive: approximately one order of magnitude more mass than what is available in a TDE scenario ( $1M_\odot$ ).

A giant flare scenario could help to resolve this issue. In the last panel of Fig. 8 and Fig. A.1–A.3 we show estimates (12) of the excited mass: they are comparable to or much larger than the typical stellar masses, see also Table 1. Fig. 9 shows the corresponding result for the most modest giant flares, obtained with a rough minimum estimate of the heated zone of the disc,  $R_{out} = R_{trunc} + z_o(R_{trunc})$ .

At the same time, in several instances, there are observations strongly suggesting that a TDE event preceded the outburst. For example, spectroscopic observations of AT 2020zso indicate the elliptical geometry of the emitter (Wevers et al. 2022), while the authors cite several previous works where emission from quasi-circular discs was reported. Further, event AT 2019azh shows signatures of both the stream-stream collision and delayed accretion (Liu et al. 2022). Linearly polarised optical emission at the level of  $\sim 25\%$  observed from AT 2020mot possibly indicate accretion disc formation, when ‘the stream of stellar material collides with itself’ (Lioudakis et al. 2023).

Figure 10 depicts the minimum truncation radius necessary for the ionization instability to trigger a giant flare versus SMBH mass. Notably, for SMBH with  $M \gtrsim 10^9 M_\odot$ , any outburst in a disc with  $\alpha_{hot} = 0.1$  and  $\alpha_{cold} = 0.01$  will be a giant flare, provided the geometrically-thin accretion disc exists at the accretion

viscous time zone’, is shrinking. In this sense, the solution for an expanding disc from Cannizzo et al. (1990) is not applicable.

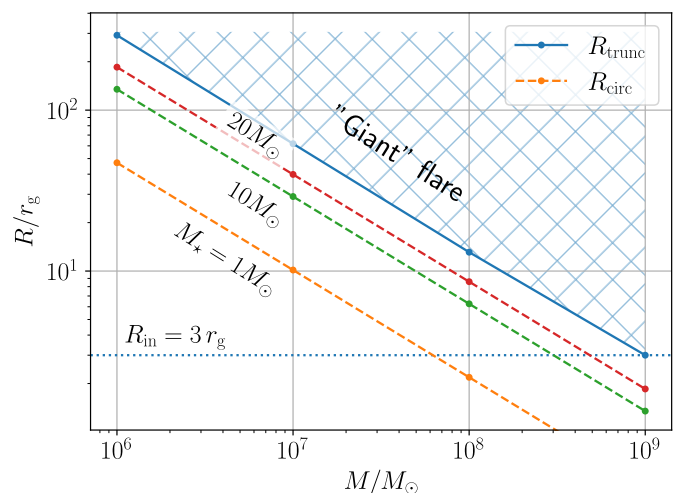


Fig. 10: Minimum ‘giant’ flare disc truncation radius and circulization radii  $R_{circ}$  for stars of 1, 10, and  $20 M_\odot$ .

rates  $\dot{M}$  less than  $10^{-5} \dot{M}_{Edd}$ . We also plot  $R_{circ}$  for stars of different masses, where dependence  $R_*(M_*)$  for the main sequence stars was used (Kippenhahn et al. 2012). It can be seen that a tidal disruption of a massive enough star can ignite a giant flare in a disc, which will increase the TDE output. This happens because the fallback material presumably forms a disc. For example, in the simulations by Andalman et al. (2022), the fallback following the complete destruction of a  $1 M_\odot$  star near a  $10^6 M_\odot$  SMBH results in a disc up to  $200r_g$ .

### 5.3. Dew cycle

The process of supplying mass to the central galactic discs during quiescent periods remains unclear (Lodato 2012; Alexander & Hickox 2012). At distances of  $\sim 0.01$  pc in the disc, the self-gravity effects such as spiral waves, fragmentation, and subsequent star formation are possible. The influence of these effects on the mass increase in the central cold disc is quite complex, as they can both nourish and hinder the feeding of SMBHs (Nayakshin et al. 2007; Hopkins & Quataert 2010). Other possible ways of feeding the central black hole have also been proposed, for example by the very low angular momentum gas (King & Pringle 2006).

Candidates for galaxies capable of producing giant flares include low-luminosity AGN (LLAGN) (Yuan & Narayan 2014) and other quiescent SMBHs (Soria et al. 2006; Volonteri et al. 2011) if a geometrically thin accretion disc manages to form at  $R \gtrsim 10 - 10^2 r_g$ . For very massive SMBH, the development of giant flares may be impossible due to the absence of a cold molecular disc, because the radius of the gravitational instability  $R_{sg}/r_g$  decreases with the increasing mass. For  $10^9 M_\odot$ , the radius  $R_{sg}$  of the self-gravity instability is less than the assumed ADAF boundary (see Fig. 7).

For low-mass stellar X-ray binaries, it is common to assume that a binary is transient, i.e. it experiences outbursts, if the transfer rate from a neighbouring star through the Lagrangian point is between  $\dot{M}^-$  and  $\dot{M}^+$ . The ratio between these values is only  $\sim 2.5$  in Fig. 2. Does this mean that only galaxies with such a rate of mass supply can have giant flares? Obviously not, since galaxies in the process of increasing their central accretion rate from very low levels could also be susceptible to giant flares.

Assuming a constant mass supply from the distant reservoir to the cold disc, the upper limit on the time between giant flares can be considered as the time required for the viscous flow in the geometrically thin disc to reach the inner radii and grow to a critical value. For the sake of estimation and order of magnitude, this can be approximated by the analytical peak time of an outburst  $t_{\text{peak}} \approx 0.1R^2/\nu_t$  (see Appendix A) which gives  $\sim 4 \times 10^5 \text{ yr} (R/100 r_g)^{3/2} (M/10^7 M_\odot)$ , where we have substituted  $z_0/R = 10^{-3}$ ,  $\alpha_{\text{cold}} = 10^{-2}$ . The radius  $R$  corresponds to the extent of the mass reservoir, which appears to be larger than  $R_{\text{trunc}}$ , but possibly only by a factor of a few to 10. If a giant flare does not reach a certain radius of the disc, this means that the mass reservoir there is intact. Consequently, the lower the estimates of the flare amplitude, the shorter the replenishment times.

However, taking into account the possibility of very complex matter supply pathways, this estimate may be far from the actual replenishment time. Note that possible events of tidal stripping of stars ('partial TDE', see Chen & Shen 2021) can significantly reduce the time between giant flares.

Given that the rate of 'complete' TDEs is estimated to be 1 event per  $10^4 - 10^5 \text{ yr}$ , see van Velzen et al. (2020); Saxton et al. (2021) and references therein, Sazonov et al. (2021); Masterson et al. (2024), we suggest that giant flares, if the mechanism is confirmed, could contribute to the observed TDE rate.

## 6. Summary

We propose a novel mechanism for outbursts associated with the ionisation-viscous instability in the accretion disc. According to our proposal, a massive, cold, neutral, geometrically thin disc with vertical convective energy transfer can transition to a slim, advection-dominated regime within a few thermal timescales, provided that the critical surface density is accumulated. The mechanism is only viable in discs around SMBH and if the turbulent parameter  $\alpha$  grows in the ionised disc.

For example, if  $\alpha_{\text{hot}} = 0.1$  and  $\alpha_{\text{cold}} = 0.01$ , and the SMBH mass is  $\geq 10^9 M_\odot$ , the giant flare can develop if the geometrically thin accretion disc exists at accretion rates  $\dot{m}$  less than  $10^{-5}$ . Also, any flare due to ionization instability in a geometrically thin convective neutral disc around SMBH with  $M \geq 10^9 M_\odot$  will be a giant flare.

For lighter SMBH, a giant outburst can develop if there is a geometrically thin accretion disc and its inner part is truncated by an optically thin, tenuous flow. An ADAF is a compelling candidate for such a scenario.

Estimated peak accretion rates depend on the size of the disc region transitioning to the ionised state and are  $\geq 10 \dot{M}_{\text{Edd}}$ , but may be somewhat reduced by the strong outflows. The characteristic outburst duration is estimated by the viscous time of a slim disc, which also depends on the size of the region involved in a flare and can range from several months to several years.

The present calculations should be considered as a rough estimate. The possibility of giant flare development needs to be further investigated using numerical models that can account for non-equilibrium processes in accretion discs.

If confirmed, giant flares could contribute to a variety of bright extragalactic phenomena, such as TDE.

## References

Abramowicz, M. A., Chen, X., Kato, S., Lasota, J.-P., & Regev, O. 1995, *ApJ*, 438, L37  
 Abramowicz, M. A., Czerny, B., Lasota, J. P., & Szuszkiewicz, E. 1988, *ApJ*, 332, 646

Alexander, D. M. & Hickox, R. C. 2012, *New A Rev.*, 56, 93  
 Andalman, Z. L., Liska, M. T. P., Tchekhovskoy, A., Coughlin, E. R., & Stone, N. 2022, *MNRAS*, 510, 1627  
 Bandopadhyay, A., Fancher, J., Athian, A., et al. 2024, *ApJ*, 961, L2  
 Bjoernsson, G., Abramowicz, M. A., Chen, X., & Lasota, J.-P. 1996, *ApJ*, 467, 99  
 Burke, C. J., Shen, Y., Blaes, O., et al. 2021, *Science*, 373, 789  
 Cannizzo, J. K., Lee, H. M., & Goodman, J. 1990, *ApJ*, 351, 38  
 Cannizzo, J. K. & Reiff, C. M. 1992, *ApJ*, 385, 87  
 Chen, J.-H. & Shen, R.-F. 2021, *ApJ*, 914, 69  
 Czerny, B. 2019, *Universe*, 5, 131  
 Czerny, B., Rózańska, A., & Kuraszkiewicz, J. 2004, *A&A*, 428, 39  
 Dai, L., McKinney, J. C., Roth, N., Ramirez-Ruiz, E., & Miller, M. C. 2018, *ApJ*, 859, L20  
 Dubus, G., Hameury, J. M., & Lasota, J. P. 2001, *A&A*, 373, 251  
 Esin, A. A., McClintock, J. E., & Narayan, R. 1997, *ApJ*, 489, 865  
 Farrar, G. R. & Gruzinov, A. 2009, *ApJ*, 693, 329  
 Faulkner, J., Lin, D. N. C., & Papaloizou, J. 1983, *MNRAS*, 205, 359  
 Hameury, J. M. 2020, *Advances in Space Research*, 66, 1004  
 Hameury, J.-M., Lasota, J.-P., & Viallet, M. 2007, in *Black Holes from Stars to Galaxies – Across the Range of Masses*, ed. V. Karas & G. Matt, Vol. 238, 297–300  
 Hameury, J.-M., Menou, K., Dubus, G., et al. 1998, *MNRAS*, 298, 1048  
 Hameury, J. M., Viallet, M., & Lasota, J. P. 2009, *A&A*, 496, 413  
 He, J. S., Dou, L. M., Ai, Y. L., et al. 2021, *A&A*, 652, A15  
 Hills, J. G. 1975, *Nature*, 254, 295  
 Hopkins, P. F. & Quataert, E. 2010, *MNRAS*, 407, 1529  
 Hung, T., Cenko, S. B., Roth, N., et al. 2019, *ApJ*, 879, 119  
 Janiuk, A. & Czerny, B. 2011, *MNRAS*, 414, 2186  
 Janiuk, A., Czerny, B., Siemiginowska, A., & Szczerba, R. 2004, *ApJ*, 602, 595  
 Jiang, Y.-F., Blaes, O., Stone, J. M., & Davis, S. W. 2019, *ApJ*, 885, 144  
 Kankare, E., Kotak, R., Mattila, S., et al. 2017, *Nature Astronomy*, 1, 865  
 Kara, E., Dai, L., Reynolds, C. S., & Kallman, T. 2018, *MNRAS*, 474, 3593  
 Kato, S., Fukue, J., & Mineshige, S. 2008, *Black-Hole Accretion Disks — Towards a New Paradigm* —  
 Kelly, B. C., Bechtold, J., & Siemiginowska, A. 2009, *ApJ*, 698, 895  
 Ketsaris, N. A. & Shakura, N. I. 1998, *Astronomical and Astrophysical Transactions*, 15, 193  
 King, A. R. & Pringle, J. E. 2006, *MNRAS*, 373, L90  
 Kippenhahn, R., Weigert, A., & Weiss, A. 2012, *Stellar Structure and Evolution*  
 Komossa, S. 2015, *Journal of High Energy Astrophysics*, 7, 148  
 Landry, R., Dodson-Robinson, S. E., Turner, N. J., & Abram, G. 2013, *ApJ*, 771, 80  
 Lasota, J.-P. 2001, *New A Rev.*, 45, 449  
 Lasota, J.-P. 2016, in *Astrophysics and Space Science Library*, Vol. 440, *Astrophysics of Black Holes: From Fundamental Aspects to Latest Developments*, ed. C. Bambi, 1  
 Lasota, J. P., Vieira, R. S. S., Sądowski, A., Narayan, R., & Abramowicz, M. A. 2016, *A&A*, 587, A13  
 Lightman, A. P. & Eardley, D. M. 1974, *ApJ*, 187, L1  
 Lin, D., Guillochon, J., Komossa, S., et al. 2017, *Nature Astronomy*, 1, 0033  
 Liodakis, I., Koljonen, K. I. I., Blinov, D., et al. 2023, *Science*, 380, 656  
 Lipunova, G. V. 1999, *Astronomy Letters*, 25, 508  
 Lipunova, G. V. 2015, *ApJ*, 804, 87  
 Liu, X.-L., Dou, L.-M., Chen, J.-H., & Shen, R.-F. 2022, *ApJ*, 925, 67  
 Lodato, G. 2012, *Advances in Astronomy*, 2012, 846875  
 Lynden-Bell, D. & Pringle, J. E. 1974, *MNRAS*, 168, 603  
 Martin, R. G., Nixon, C. J., Pringle, J. E., & Livio, M. 2019, *New A*, 70, 7  
 Masterson, M., De, K., Panagiotou, C., et al. 2024, *ApJ*, 961, 211  
 Matsumoto, T. & Piran, T. 2021, *MNRAS*, 502, 3385  
 Menou, K. & Quataert, E. 2001a, *ApJ*, 562, L137  
 Menou, K. & Quataert, E. 2001b, *ApJ*, 552, 204  
 Metzger, B. D. & Stone, N. C. 2016, *MNRAS*, 461, 948  
 Meyer, F. 1984, *A&A*, 131, 303  
 Meyer, F. & Meyer-Hofmeister, E. 1981, *A&A*, 104, L10  
 Meyer, F. & Meyer-Hofmeister, E. 2015, *PASJ*, 67, 52  
 Mineshige, S. & Shields, G. A. 1990, *ApJ*, 351, 47  
 Narayan, R. 1996, *ApJ*, 462, 136  
 Narayan, R. & McClintock, J. E. 2008, *New A Rev.*, 51, 733  
 Narayan, R. & Yi, I. 1994, *ApJ*, 428, L13  
 Nayakshin, S., Cuadra, J., & Springel, V. 2007, *MNRAS*, 379, 21  
 Nemmen, R. S., Storchi-Bergmann, T., & Eracleous, M. 2014, *MNRAS*, 438, 2804  
 Penna, R. F., Sądowski, A., Kulkarni, A. K., & Narayan, R. 2013, *MNRAS*, 428, 2255  
 Piran, T. 1978, *ApJ*, 221, 652  
 Poutanen, J., Krolik, J. H., & Ryde, F. 1997, *MNRAS*, 292, L21  
 Poutanen, J., Lipunova, G., Fabrika, S., Butkevich, A. G., & Abolmasov, P. 2007, *MNRAS*, 377, 1187  
 Rees, M. J. 1988, *Nature*, 333, 523

- Safronov, V. S. 1960, *Annales d'Astrophysique*, 23, 979
- Sarin, N. & Metzger, B. D. 2024, *ApJ*, 961, L19
- Saxton, R., Komossa, S., Auchettl, K., & Jonker, P. G. 2021, *Space Sci. Rev.*, 217, 18
- Sazonov, S., Gilfanov, M., Medvedev, P., et al. 2021, *MNRAS*, 508, 3820
- Shakura, N. I., Lipunova, G. V., Malanchev, K. L., et al. 2018, *Accretion flows in astrophysics* (New York: New York)
- Shakura, N. I. & Sunyaev, R. A. 1973, *A&A*, 500, 33
- Shakura, N. I. & Sunyaev, R. A. 1976, *MNRAS*, 175, 613
- Shen, R.-F. & Matzner, C. D. 2014, *ApJ*, 784, 87
- Siemiginowska, A. & Czerny, B. 1989, *MNRAS*, 239, 289
- Siemiginowska, A., Czerny, B., & Kostyunin, V. 1996, *ApJ*, 458, 491
- Smak, J. 1984a, *Acta Astron.*, 34, 161
- Smak, J. 1984b, *PASP*, 96, 5
- Śniegowska, M., Czerny, B., Bon, E., & Bon, N. 2020, *A&A*, 641, A167
- Śniegowska, M., Grzędzielski, M., Czerny, B., & Janiuk, A. 2023, *A&A*, 672, A19
- Soria, R., Graham, A. W., Fabbiano, G., et al. 2006, *ApJ*, 640, 143
- Starling, R. L. C., Siemiginowska, A., Uttley, P., & Soria, R. 2004, *MNRAS*, 347, 67
- Tavleev, A. S., Lipunova, G. V., & Malanchev, K. L. 2023, *MNRAS*, 524, 3647
- Toomre, A. 1964, *ApJ*, 139, 1217
- Ulmer, A. 1999, *ApJ*, 514, 180
- van Velzen, S., Holoien, T. W. S., Onori, F., Hung, T., & Arcavi, I. 2020, *Space Sci. Rev.*, 216, 124
- Volonteri, M., Dotti, M., Campbell, D., & Mateo, M. 2011, *ApJ*, 730, 145
- Wevers, T., Nicholl, M., Guolo, M., et al. 2022, *A&A*, 666, A6
- Xie, Z. H., Ma, L., Zhang, X., et al. 2009, *ApJ*, 707, 866
- Yan, Z. & Xie, F.-G. 2018, *MNRAS*, 475, 1190
- Yuan, F. & Narayan, R. 2014, *ARA&A*, 52, 529
- Zhang, X. 2023, *ApJ*, 948, 68

*Acknowledgements.* We thank Arman Tursunov for comments on the manuscript. We acknowledge the usage of computing resources of the M. V. Lomonosov Moscow State University Program of Development. Support was provided by Schmidt Sciences, LLC. for KM.

## Appendix A: Analytic relations for $e$ -folding time and peak accretion rate

Lipunova (2015) shows that the  $e$ -folding decay time of the accretion rate evolution in a finite disc with constant viscosity<sup>3</sup> is related to the viscous time as follows:

$$t_{\text{exp}} = \frac{16 l^2}{3 k_1^2} \frac{R_{\text{out}}^2}{\nu_t(R_{\text{out}})}, \quad (\text{A.1})$$

where  $l$  is the parameter defined by the viscosity type, introduced by Lynden-Bell & Pringle (1974) and  $k_1$  depends on the boundary conditions (Lipunova 2015) and lies in the interval 1 – 1.6 for many cases of accreting discs.

The peak accretion rate in the solution of Lynden-Bell & Pringle (1974) for the infinite disc is

$$\dot{M}_{\text{peak}} = \frac{M_{\text{disc}}}{t_{\text{peak}}} \frac{(1+l)^l}{e^{1+l} \Gamma(l)} \quad (\text{A.2})$$

with

$$t_{\text{peak}} = \frac{4}{3} \frac{l^2}{(1+l)} \frac{R_{\text{out}}^2}{\nu_t}. \quad (\text{A.3})$$

(see Appendix of Lipunova 2015).

Combining above formulae, we arrive at

$$\dot{M}_{\text{peak}} = \frac{M_{\text{disc}}}{R_{\text{out}}^2/\nu_t} \frac{3(1+l)^{1+l}}{4 l^2 e^{1+l} \Gamma(l)} = C \frac{M_{\text{disc}}}{R_{\text{out}}^2/\nu_t} \quad (\text{A.4})$$

with  $C \approx 0.97$  for  $l = 1/3$ , appropriate for discs with constant semi-thickness. For such discs, the dimensionless factor in (A.1) is about 0.4.

Following the vertical structure solution, we employ

$$t_{\text{vis}} = \frac{R_{\text{out}}^2}{\nu_t(R_{\text{out}})} = \frac{3}{2} \frac{1}{\alpha \omega_K} \left( \frac{z_0}{r} \right)^{-2} \Pi_1 \quad (\text{A.5})$$

and substitute  $\Pi_1 = 6$  (see Shakura et al. 2018, §1.5.2 and equation 1.148).

Figures A.1–A.3 show the same flare characteristics as Fig. 8 for other considered masses of SMBH. They are calculated according to the scheme described in §4 and using the critical surface densities, which could be viewed for different masses in Fig. A.4.

In Figure A.4, for  $10^8$  and  $10^9 M_{\odot}$ , the stationary distributions  $\Sigma_{\text{stat}}(r)$  are plotted only for  $r < R_{\text{sg}}$  defined by (10). For these SMBH masses, critical  $\Sigma^+$  cannot be found for large  $r$  because the positive hot geometrically thin branch of the S-curve disappears. In this case the values  $\Sigma_A$  and  $\Sigma_{\text{adv}}$ , which require  $\Pi_{1,4}$  at a point on this branch, are extrapolated from smaller radii. These intervals are shown as transparent in the lower panels of Fig. A.4. The extrapolated values affect only the flare characteristics calculated if  $R_{\text{out}} = R_{\text{out,max}}$ .

<sup>3</sup> For spatially confined accretion disc with varying viscosity  $\nu_t$ , evolution is described by a power-law dependence on time but can be approximated by exponential for a limited time interval.

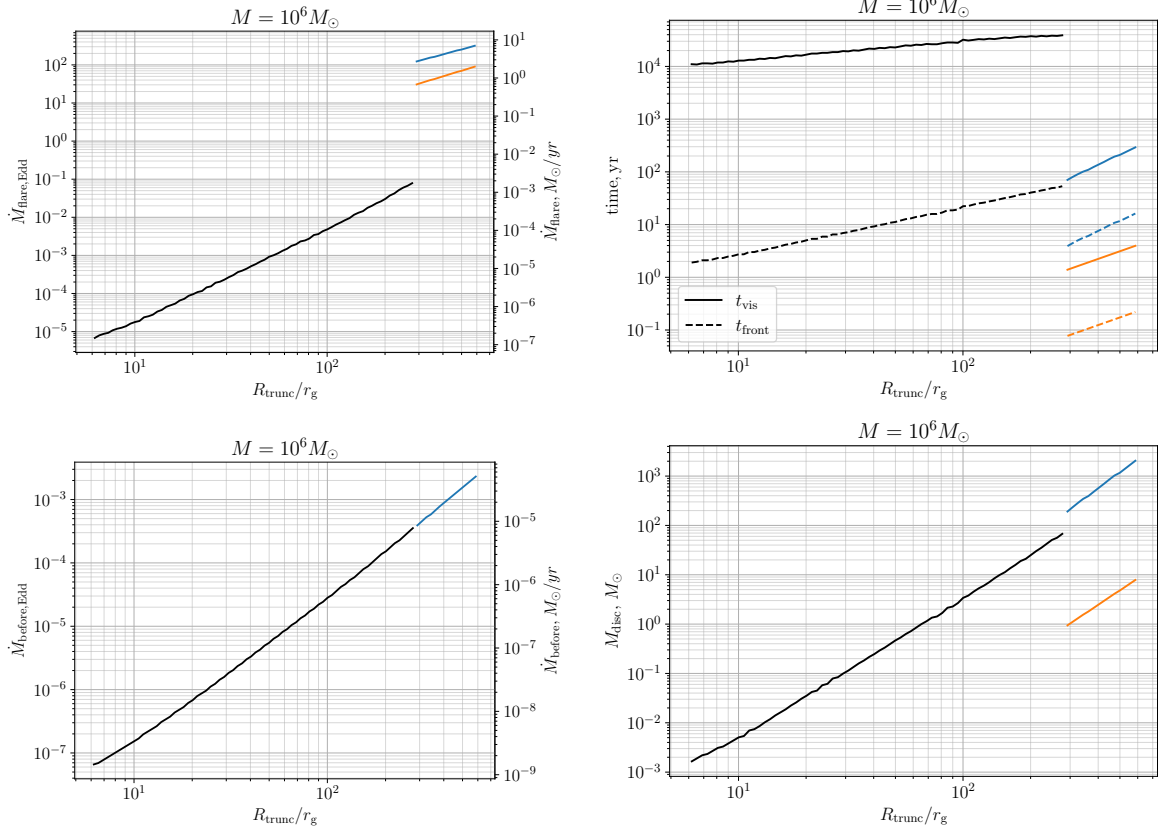


Fig. A.1: Same as Fig. 8 but for  $10^6 M_\odot$ .

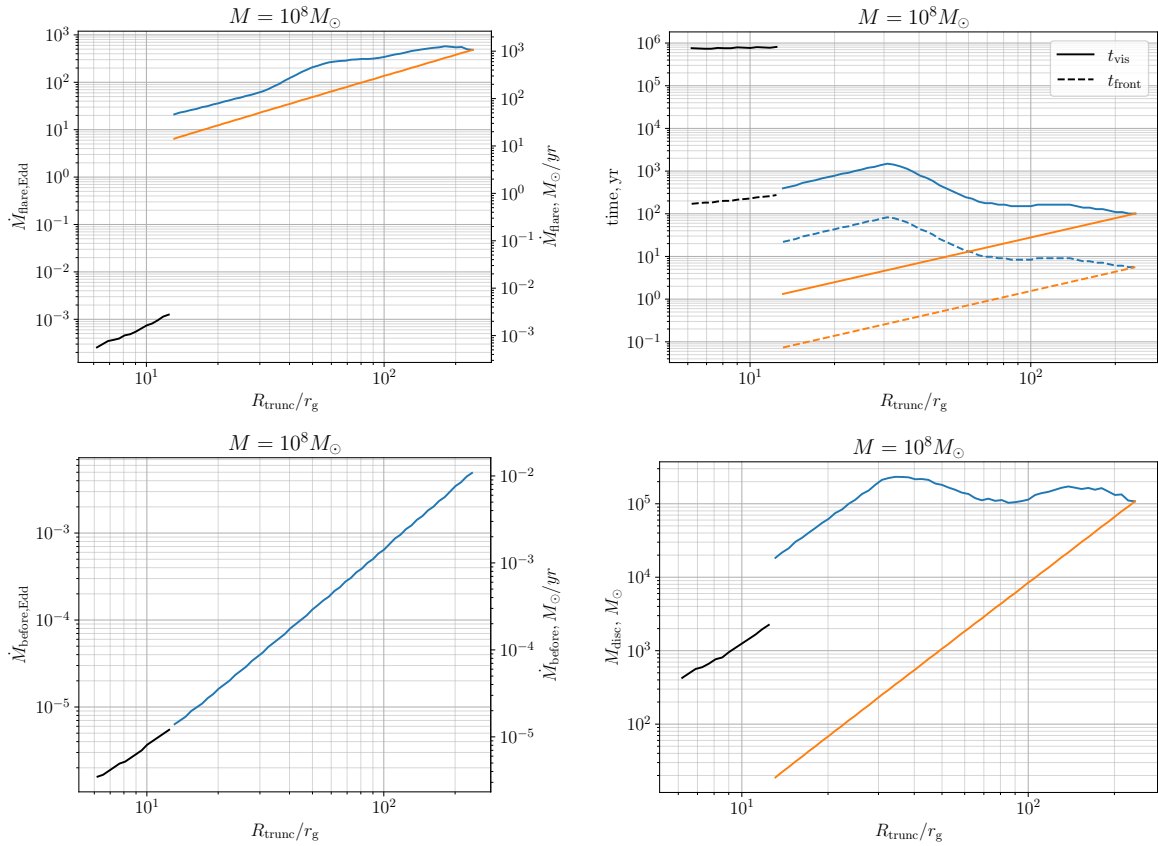


Fig. A.2: Same as Fig. 8 but for  $10^8 M_\odot$ .

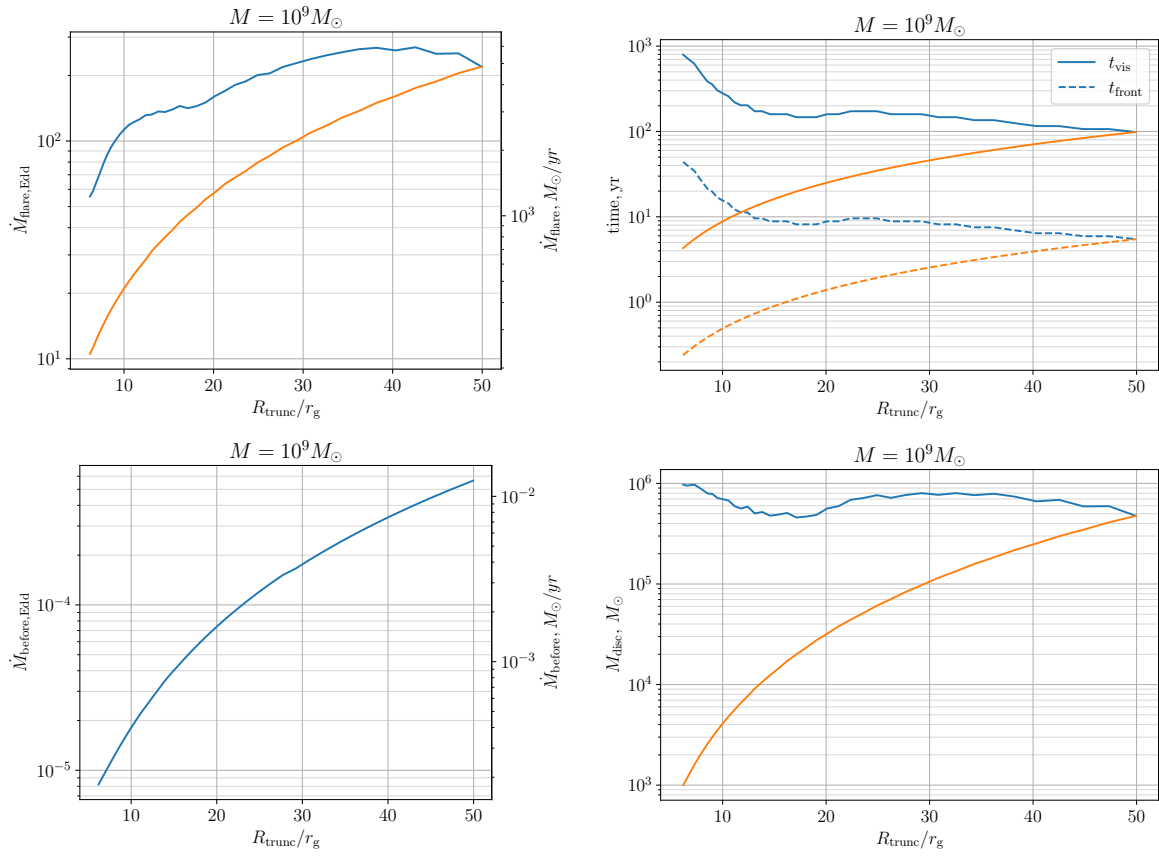


Fig. A.3: Same as in Fig. 8, but for  $10^9 M_\odot$ . For all  $R_{\text{trunc}}$ , the flare will be giant. The quiescent disc is limited at large radii according to the condition of self-gravitational instability.

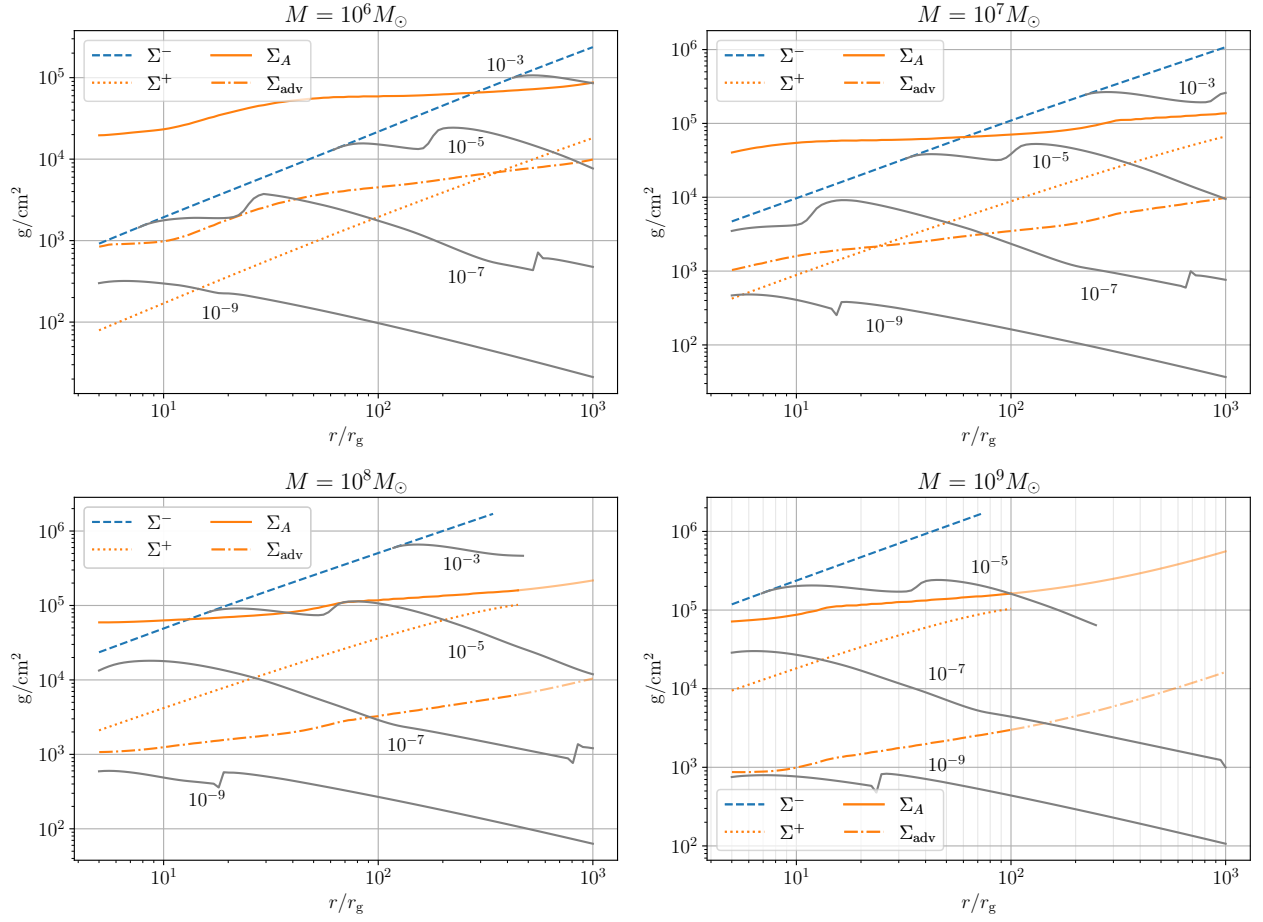


Fig. A.4: Radial distributions of  $\Sigma^-$ ,  $\Sigma_A$ ,  $\Sigma^+$ , and  $\Sigma_{\text{adv}}$  for different masses of central BH, see (8). Also shown is the stationary distribution  $\Sigma_{\text{stat}}$  (grey lines) for different  $\dot{M}$  (in  $\dot{M}_{\text{Edd}}$  units) for  $\alpha_{\text{cold}} = 0.01$ . See description in §2.2 and Appendix A.